Mycobacterium tuberculosis Type VII Secreted Effector EsxH Targets Host ESCRT to Impair Trafficking

Citation	Mehra, A., A. Zahra, V. Thompson, N. Sirisaengtaksin, A. Wells, M. Porto, S. Köster, et al. 2013. "Mycobacterium tuberculosis Type VII Secreted Effector EsxH Targets Host ESCRT to Impair Trafficking." PLoS Pathogens 9 (10): e1003734. doi:10.1371/journal.ppat.1003734. http://dx.doi.org/10.1371/journal.ppat.1003734.
Published Version	doi:10.1371/journal.ppat.1003734
Accessed	February 19, 2015 2:53:31 PM EST
Citable Link	http://nrs.harvard.edu/urn-3:HUL.InstRepos:11879172
Terms of Use	This article was downloaded from Harvard University's DASH repository, and is made available under the terms and conditions applicable to Other Posted Material, as set forth at http://nrs.harvard.edu/urn-3:HUL.InstRepos:dash.current.terms-of-use#LAA

(Article begins on next page)

PLOS | PATHOGENS

Mycobacterium tuberculosis Type VII Secreted Effector EsxH Targets Host ESCRT to Impair Trafficking

Alka Mehra[1][9], Aleena Zahra[1][9], Victor Thompson[1], Natalie Sirisaengtaksin[2], Ashley Wells[1], Maura Porto[1], Stefan Köster[1], Kristen Penberthy[1], Yoshihisha Kubota[2], Amelie Dricot[3,4], Daniel Rogan[1], Marc Vidal[3,4], David E. Hill[3,4], Andrew J. Bean[2,5], Jennifer A. Philips[1]*

1 Division of Infectious Diseases, Department of Medicine, Department of Pathology and Department of Microbiology, New York University School of Medicine, New York, New York, United States of America, 2 Department of Neurobiology and Anatomy, and Graduate School of Biomedical Sciences, The University of Texas Health Science Center at Houston, Houston, Texas, United States of America, 3 Center for Cancer Systems Biology (CCSB) and Department of Cancer Biology, Dana-Farber Cancer Institute, Boston, Massachusetts, United States of America, 4 Department of Genetics, Harvard Medical School, Boston, Massachusetts, United States of America, 5 Division of Pediatrics, The University of Texas M.D. Anderson Cancer Center, Houston, Texas, United States of America

Abstract

Mycobacterium tuberculosis (Mtb) disrupts anti-microbial pathways of macrophages, cells that normally kill bacteria. Over 40 years ago, D'Arcy Hart showed that Mtb avoids delivery to lysosomes, but the molecular mechanisms that allow Mtb to elude lysosomal degradation are poorly understood. Specialized secretion systems are often used by bacterial pathogens to translocate effectors that target the host, and Mtb encodes type VII secretion systems (TSSSs) that enable mycobacteria to secrete proteins across their complex cell envelope; however, their cellular targets are unknown. Here, we describe a systematic strategy to identify bacterial virulence factors by looking for interactions between the Mtb secretome and host proteins using a high throughput, high stringency, yeast two-hybrid (Y2H) platform. Using this approach we identified an interaction between EsxH, which is secreted by the Esx-3 TSSS, and human hepatocyte growth factor-regulated tyrosine kinase substrate (Hgs/Hrs), a component of the endosomal sorting complex required for transport (ESCRT). ESCRT has a well-described role in directing proteins destined for lysosomal degradation into intraluminal vesicles (ILVs) of multivesicular bodies (MVBs), ensuring degradation of the sorted cargo upon MVB-lysosome fusion. Here, we show that ESCRT is required to deliver Mtb to the lysosome and to restrict intracellular bacterial growth. Further, EsxH, in complex with EsxG, disrupts ESCRT function and impairs phagosome maturation. Thus, we demonstrate a role for a TSSS and the host ESCRT machinery in one of the central features of tuberculosis pathogenesis.

Competing Interests: The authors have declared that no competing interests exist.

* E-mail: Jennifer.Philips@nyumc.org

[9] These authors contributed equally to this work.

Introduction

An important virulence property of *Mycobacterium tuberculosis* (Mtb)- the causative agent of the disease tuberculosis- is its ability to avoid delivery to the lysosome. It has long been appreciated that Mtb alters phagosome maturation, such that internalized bacteria are not transported to the lysosome but instead reside in an early endosome-like compartment [1,2]. The Mtb-induced block in phagosome-lysosome fusion has been attributed to a wide array of lipid and protein effectors [3,4] but the mechanism remains poorly understood. More recently, the ability of Mtb to permeabilize the phagosomal membrane, which allows bacterial products and in some cases intact bacteria to access the cytosol, has been described [5–9]. The TSSS Esx-1 and its secreted effectors, EsxA/ESAT-6 and EsxB/CFP-10, are critical for this process. Esx-1 has been investigated intensively because its absence in the vaccine strain

Mycobacterium bovis-BCG (BCG) largely accounts for attenuation of that strain [8–10]. Mtb encodes five loci resembling Esx-1 (Esx-1-Esx-5), as well as 11 tandem pairs of proteins similar to EsxA and EsxB (EsxA-EsxW), but their cellular targets, if any, are unknown [11]. Esx-3 plays a role in iron acquisition in Mtb, as well as in a non-pathogenic strain, *Mycobacterium smegmatis* (Msmeg) [12,13]. Esx-3 is a focus of vaccine efforts because it secretes EsxG/TB9.8 and EsxH/TB10.4, which are highly antigenic [14,15], and because introduction of the Mtb ESX-3 locus into an Msmeg strain lacking the endogenous ESX-3 region generates highly protective immunity [16]. The ESX-5 locus is required for transport of proteins with conserved proline-glutamic acid (PE) and proline-proline-glutamic acid (PPE) motifs [17,18] and modulates macrophage responses [19]. Thus, TSSSs and their putative effectors appear to be important in virulence and modulating host cells, however, their mechanism of action and molecular targets are unclear.

Author Summary

Mycobacterium tuberculosis (Mtb) causes the disease tuberculosis, one of the world's most deadly infections. The host immune system can't eradicate Mtb because it grows within macrophages, cells that normally kill bacteria. One of the intracellular survival strategies of Mtb is to avoid delivery to lysosomes, a phenomenon described over 40 years ago, but for which the mechanism and molecular details remain incomplete. Mtb possess specialized secretion systems (Type VII secretion systems; TSSS) that transfer particular proteins out of the bacteria, but how these proteins promote infection is not well understood. In this study, we used a high stringency yeast two-hybrid system to identify interactions between secreted effectors from Mtb and human host factors. We identified ninety-nine such interactions and focused our attention on the interaction between EsxH, secreted by Esx-3, a TSSS of Mtb, and Hrs, a component of the host ESCRT machinery. We provide evidence that Mtb EsxH directly targets host Hrs to disrupt delivery of bacteria to lysosomes. Thus, this study demonstrates the role of a TSSS effector and the ESCRT machinery in what is one of the central features of tuberculosis pathogenesis, thereby providing molecular insight into why humans can't clear Mtb infection.

Here, we show that EsxG and EsxH from Mtb, but not the Msmeg homologs, target the host factor, Hrs. Hrs is a component of the ESCRT machinery, a group of four protein complexes (ESCRT-0 to ESCRT-III) composed of cytosolic components that are sequentially recruited to the endosomal membrane. The ESCRT machinery has a well-described role in directing cargo destined for degradation into intraluminal vesicles of multivesicular bodies (MVBs) that fuse with lysosomes [20,21]. We show that ESCRT is also required to deliver Mtb to the lysosome and to restrict intracellular bacterial growth. EsxH, in complex with EsxG, is able to disrupt ESCRT function and impair phagosome maturation.

Results

High throughput identification of Mtb secretome-human host interactions

We used a systematic strategy to identify secreted bacterial virulence factors by looking for interactions with host proteins using a high throughput, high stringency, yeast two-hybrid (Y2H) platform [22]. First, we curated the literature to define the Mtb secretome. Thirty-eight publications predicted 718 secreted proteins based on presence in culture filtrate (CF), ability to cause secretion of an assayable protein, bioinformatic criteria, or detailed study (see Text S1 for additional details). In order to prioritize open reading frames (ORFs) for screening, we imposed a number of criteria, such as excluding proteins with multiple transmembrane spanning domains (see Text S1 for additional details). In addition, since the starting list of putative secreted proteins might contain proteins that are not actually secreted, we attempted to eliminate ORFs that were likely to be inaccurately classified as secreted. One way in which this can happen is if cytoplasmic proteins appear in CF due to bacterial lysis. In order to minimize the contribution of such proteins, we did not include ORFs that were annotated in Tuberculist (http://tuberculist.epfl.ch/) as being involved in lipid metabolism, information pathways (which contains proteins involved in replication, transcription and translation), or intermediary metabolism and respiration, since

most of these are likely involved in basic, intrinsic bacterial processes, and hence, many may be misclassified. To avoid removing true secreted proteins, ORFs were not de-prioritized if they had a possible signal sequence or there were data supporting their role during infection. In doing so, we removed many proteins that were found in CF in a single study, and hence may be misclassified (see Text S1 for details). From the final list, 339 sequence validated secretome ORFs were provided by Pathogen Functional Genomic Resource Center (PFGRC; Dataset S1). Because many secreted proteins play an intrinsic role in the bacterial lifecycle, we anticipated that only a small fraction would interact with human proteins. Thus, to estimate a false positive hit rate of our system, we included sixty ORFs that are not likely to be secreted to serve as controls (see Text S1 for details; Dataset S2).

In order to evaluate their performance in Y2H protein-protein interaction (PPI) mapping, we tested the 399 Mtb ORFs expressed as Gal4-DNA binding domain (DB) fusions for pair wise interactions with the same 399 Mtb ORFs expressed as Gal4-activation domain (AD) fusions. From the ~160,000 combinations queried, we found 14 unique PPIs (Table S1). The rate of interactions is as high as in human ORFeome mapping [22], exceeding the stochastic false positive rate of the Y2H platform by fifteen-fold [23]. Half of the interactions were between proteins belonging to the WXG100 family (EssA-EsxW). These proteins are approximately 100 amino acids in length and have a characteristic hairpin bend formed by a Trp-Xaa-Gly (W-X-G) motif. Mtb encodes 11 tandem pairs of such proteins, which are thought to function as secreted heterodimers. Heterodimer formation is proposed to be limited to interactions between genome pairs or very closely related family members [24,25], and the interactions we detected by Y2H exhibit this specificity. Six of the remaining seven PPIs involved homotypic interactions; for example, bacterioferritin (BfrB) was found to interact with itself, consistent with the proposal that it assembles into 24-subunit oligomers [26].

After ensuring the high performance of Mtb ORFs in Y2H PPI mapping, we looked for interactions between the Mtb secretome and ~12,000 human ORFs, testing approximately 4 million interactions. From the secretome collection, we identified 99 PPIs between 53 Mtb proteins and 63 human proteins (Dataset S3). The number of Mtb proteins exhibiting an interaction with a human protein was approximately two-fold higher for the secretome collection compared to the non-secreted control set (53 out of 339 versus 5 out of 60). We analyzed the collection to determine whether PPIs were enriched for subsets of Mtb proteins (Table S2). We observed that the sixteen Esx proteins included in the collection were significantly more likely to interact with human ORFs than were controls (p = 0.0087). The finding that Esx proteins were enriched for interactions may reflect that this group of proteins plays an important role in virulence, or could mean that these proteins, which usually form a heterodimer, are prone to aberrant interactions when they are expressed without their binding partner.

It is difficult to gauge the success of the screen based upon known interaction between Mtb proteins and cytosolic human protein because so few are known. Included in our screening set were, PtpA, which has been shown to interact with Vps33B and the H subunit of the human v-ATPase [27,28], LpdC, which interacts with coronin 1 [29], and NdkA, which interacts with Rab5 and Rab7 [30]. We did not identify these known interactions, however, the screen was not performed to saturation and the Y2H platform can detect ~20% of well-validated interacting pairs [31]. We did identify an interaction between PtpA and Ligand of Numb protein X (LNX1), a RING finger-type

E3 ligase that contains 4 PDZ domains and plays a scaffolding role in diverse cellular pathways. Several other secretome ORFs also interacted with LNX1, suggesting that LNX1 might be modulated by Mtb, or LNX1 might regulate the function or stability of certain Mtb effectors.

When we examined hit rates based upon the functional category of the Mtb ORFs, the category with the greatest enrichment was cell wall and cell processes, which contains the Esx family members. The intermediary metabolism and respiration category exhibited a hit rate similar to the control collection, consistent with the idea that most of these ORFs do not function in host interactions as their annotation suggests. Interestingly, one of the two proteins that did exhibit an interaction in this category is Zmp1, a zinc metalloprotease which has been shown to inhibit the inflammasome and impair phagosome maturation but whose cellular target is unknown [32]. Zmp1 interacted with KCTD6, a BTB/POZ domain containing protein that can function as a Cullin3 (Cul3) adaptor [33]. Cul3 has recently been shown to be a regulator of endo-lysosomal trafficking, suggesting that Zmp1 may impair phagosome maturation by acting on KCTD6-Cul3 [34].

To evaluate the human targets of the Mtb proteins, we searched the STRING database (http://string.embl.de/) for each of the proteins' functional associations. The STRING database predicts protein-protein interactions based upon physical and functional associations, such as available high-throughput data, co-expression, genomic context, and text mining of available literature. Using a medium confidence value to define protein-protein interactions, there were significantly more interactions (n = 16) observed for the human targets than would be predicted by chance (p = 8.3×10^{-12}). We identified proteins involved in host immunity to bacterial infection, such as Ndp52 [35,36], Tax1pb1 [37], and STAT3 [38], however, human targets of the Mtb proteins were not significantly enriched for annotated pathways in the Kyoto Encyclopedia of Genes and Genomes (KEGG) when corrected for multiple testing, which may reflect the limited number of human targets found.

ESCRT is required for restricting intracellular growth and trafficking of slow growing mycobacteria

We focused on the interaction between EsxH and Hrs because TSSSs, which secrete Esx proteins, are clearly important in virulence but the function of their secreted effectors is largely unknown. In addition, our existing data supported the idea that the ESCRT machinery is important in controlling bacterial replication. Hrs, which plays a central role in the assembly of the initial ESCRT components on endosomes, is recruited to mycobacterial phagosomes [39], and we had previously shown in an RNAi screen in *Drosophila* that ESCRT restricts the intracellular growth of rapidly growing mycobacteria [40,41]. Control of bacterial replication appears to be particularly sensitive to ESCRT perturbation, because, in addition, when we screened ~6500 siRNA pools in RAW 264.7 (RAW) macrophages for their ability to confer enhanced intracellular growth of Msmeg, we found that the two strongest hits were Rab7, known to be involved in late endosome-lysosome fusion, and Tsg101, an ESCRT-I component that is recruited to endosomes by Hrs (data not shown). Hrs was also identified in this screen, although previously we had found no effect with Hrs silencing, which we now attribute to insufficient protein depletion [41]. In the RAW cell RNAi screen that identified Hrs, we used Ambion Silencer siRNA pools, whereas previously we used a Dharmacon siGENOME pool to deplete Hrs [41]. To clarify the discrepancy, we tested a third pool (Dharmacon ON-TARGET*plus*), which, like the Ambion pool,

conferred enhanced growth to Msmeg. We tested the individual Dharmacon ON-TARGET*plus* siRNAs and found that 2 of 4 targeting Hrs resulted in depletion of Hrs protein, enhanced the growth of Msmeg, and altered trafficking, whereas the other two had no effect (Figure S1 and data not shown). Thus, one possibility is that Mtb secretes EsxH, which binds Hrs and impairs ESCRT function, thereby promoting intracellular bacterial growth. To determine whether ESCRT restricts growth of Mtb, we depleted Hrs and Tsg101 and examined the intracellular growth of Mtb in RAW macrophages. We found no significant effect of silencing on bacterial uptake (data not shown), however when we assessed bacterial colony forming units (CFU) two day post-infection, we observed enhanced intracellular survival of Mtb in cells depleted of Hrs or Tsg101, similar to what was seen with Rab7 silencing (Figure 1A). Intracellular growth of BCG in bone marrow-derived macrophages (BMDMs) was even more strongly effected (Figure S2). Thus, Hrs restricts growth of slow growing and virulent mycobacteria.

ESCRT targets certain cell surface receptors and biosynthetic cargo to lysosomes [42]. Thus, ESCRT might restrict intracellular bacterial growth by governing bacterial trafficking and/or lysosomal content. We examined the localization of Mtb relative to Transferrin Receptor (TfR), a marker of early and recycling endosomes, and LAMP1, a marker of late endosomes and lysosomes using automated image analysis (Figures S3A, S3B). In cells depleted of Tsg101, Hrs, or Rab7, we observed diminished co-localization between Mtb and LAMP1 and a concomitant increase in co-localization of Mtb with TfR compared to control cells 24 hours post-infection (hpi) (Figure 1B), suggesting decreased Mtb delivery to degradative compartments. Similarly, in cells infected with BCG there was diminished co-localization with LysoTracker, which accumulates in the acidic environment of the lysosome, and enhanced co-localization with TfR (Figure 1B). Thus, Hrs and Tsg101, like Rab7, are required for bacterial trafficking. To verify that bacterial viability correlates with low LAMP1 and LysoTracker co-localization and with high TfR co-localization, we compared the cellular localization of viable bacteria to total bacteria. We identified metabolically active BCG 24 hpi based upon their ability to induce expression of GFP from a tetracycline-inducible promoter (BCG-tet-GFP) and compared their intracellular localization to the BCG strain that constitutively express GFP (BCG-GFP). Whereas there was a wide range in intensities of associated LAMP1 and LysoTracker with BCG-GFP, metabolically active bacteria were found almost exclusively in phagosomes with minimal acidification, little co-localization with LAMP1, and enhanced TfR co-localization at 48 hpi (Figure S3C). Thus, impaired bacterial trafficking to a late endosomal or lysosomal compartment underlies the failure to control mycobacterial replication in ESCRT-depleted cells, although altered lysosomal content may also contribute.

The Mtb EsxG EsxH heterodimer binds Hrs

Pathogenic mycobacteria arrest phagosome maturation in evolutionarily diverse cells. Supporting the idea that EsxH might play a role in inhibition of bacterial degradation, we observed that EsxH interacts with human, mouse, and zebrafish orthologs of Hrs, suggesting that it recognizes a conserved structural feature of Hrs (Figure 2A). Orthologs of EsxH are found widely in mycobacteria, including in the non-pathogen Msmeg. If EsxH prevents phagosome-lysosome fusion by impairing Hrs function, we anticipate that would be a feature specific to EsxH from pathogenic mycobacteria. To test this, we cloned the EsxH ortholog from Msmeg (MSMEG_0621; EsxH$_{Ms}$), which encodes a protein 75% identical to EsxH from Mtb (hereafter referred to as
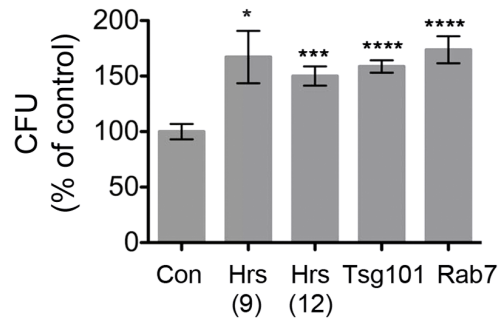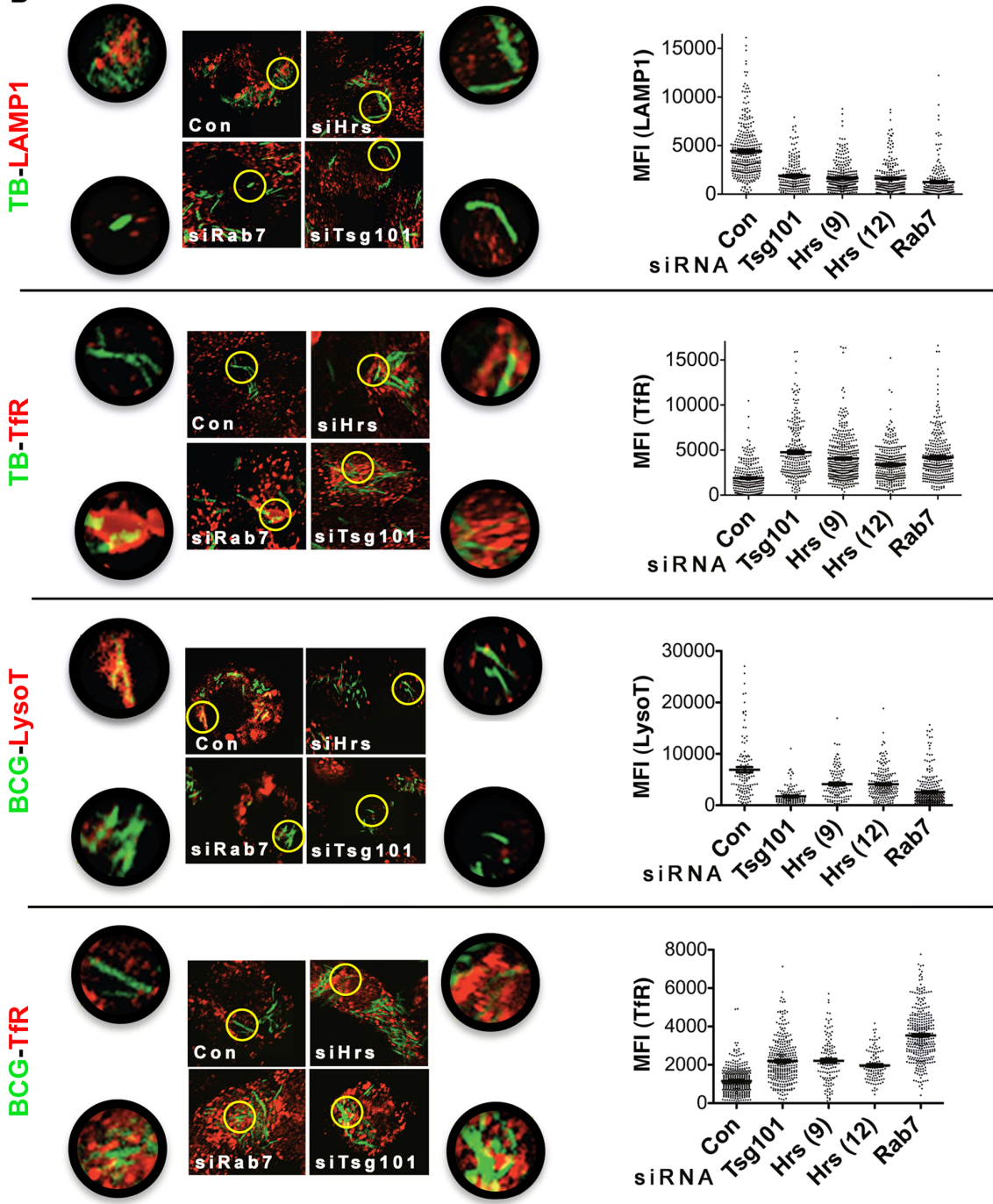
Figure 1. ESCRT is required to traffic Mtb to the lysosome. (A) RAW264.7 cells were treated with control siRNA (Con), individual siRNAs targeting Hrs (#9 or #12), or siRNA pools targeting Tsg101 or Rab7 and infected with Mtb. Bacterial colony forming units (CFU) were enumerated 2 d post-infection and are normalized to the average number of CFU in control wells from three independent experiments. Results reflect the mean +/− SEM. *$p = 0.018$; ***$p = 0.0002$; ****$p < 0.0001$, unpaired Student's t-test. (B) Composite images and quantification of Mtb-GFP or BCG-GFP (in green) and RAW cell LAMP1, TfR, or LysoTracker (in red) at 24 hpi. Regions indicated by yellow circles are shown in higher magnification in adjacent panels. In graphs, data points are the mean fluorescence intensity (MFI) around at least 100 phagosomes for each condition; bars show mean +/− SEM. Data are representative of at least three experiments; $p < 0.0001$ for all siRNAs compared to controls.
doi:10.1371/journal.ppat.1003734.g001

EsxH$_{Mt}$). Although EsxH$_{Ms}$ interacted with EsxG$_{Mt}$, demonstrating that the protein was functional in the Y2H assay, it interacted poorly with Hrs (Figure 2A), consistent with the notion that the interaction of EsxH$_{Mt}$ with Hrs contributes to virulence.

EsxH$_{Mt}$ forms a heterodimer with EsxG$_{Mt}$, composed of a four-helix bundle with flexible N- and C-terminal arms from both proteins that coordinate zinc and contribute to a cleft that has been predicted to mediate a PPI [43]. To determine whether Hrs interacts with the heterodimer, we used a fusion protein in which EsxG$_{Mt}$ and EsxH$_{Mt}$ were expressed as a single polypeptide that preserves the folded structure of the native heterodimer [44]. This fusion protein interacted with Hrs (Figure 2B). Deletion of the first five amino acids of EsxH$_{Mt}$ (EsxG$_{Mt}$-EsxH$_{Mt}$-ΔN5) weakened its interaction with Hrs (Figure 2B). These data show that Hrs can interact with EsxH$_{Mt}$ when it is complexed to EsxG$_{Mt}$ and suggest that the conformation of the amino terminal arm of EsxH$_{Mt}$ is important. To further test whether the structure of the N- and C-termini are important, we mutated His-14, His-70, and His-76 Glu-77. These residues contribute to zinc binding, and His-76 is also part of the predicted cleft. We mutated them to Ala, with the exception of His-70, which we changed to Arg because this is found in EsxH$_{Ms}$. While H14A and H70R did not have a detectable effect, when His-76 and Glu-77 were both changed to Ala, the interaction between EsxH$_{Mt}$ and Hrs was impaired, although EsxH$_{Mt}$ H76A-E77A still interacted with EsxG$_{Mt}$ (Figure 2A). To verify that EsxH$_{Mt}$ binds Hrs, we purified the EsxG$_{Mt}$ EsxH$_{Mt}$ heterodimer from *E. coli* [44] and Hrs from baculovirus [45]. Hrs bound EsxG$_{Mt}$ EsxH$_{Mt}$ in a saturable manner, exhibiting stoichiometric binding with a Kd of ~5 μM (Figure 2C and 2D). We conclude that Hrs interacts with the EsxG$_{Mt}$ EsxH$_{Mt}$ heterodimer, and the interaction likely involves the N- and C-terminal arms of EsxH$_{Mt}$.

EsxG$_{Mt}$ and EsxH$_{Mt}$ disrupt ESCRT function in mammalian cells

To determine whether EsxH$_{Mt}$ interacts with Hrs and alters ESCRT function in mammalian cells, we expressed EsxH$_{Mt}$–FLAG in HEK293 cells. EsxH$_{Mt}$ was not detectable unless we co-expressed EsxG$_{Mt}$. (Figure 3A, compare lanes 1 and 3; see Figure S4 for quantification); its abundance was also increased slightly by overexpression of Hrs (compare lane 1' with 2' and lane 5 with 6). When expressed alone, EsxH$_{Mt}$ could be stabilized by MG132, likely because it is not properly folded without EsxG$_{Mt}$ and hence is subject to proteasome-mediated degradation (Figure 3A compare lanes 1 and 5). To determine if there was an interaction between EsxG$_{Mt}$-EsxH$_{Mt}$ and Hrs, we performed co-immunoprecipitation experiments in cells co-transfected with EsxG$_{Mt}$, EsxH$_{Mt}$, and Hrs-myc. Hrs was immunoprecipitated with an antibody directed against the myc-tag, and we found that EsxH$_{Mt}$ was co-immunoprecipitated (Figure 3B). No EsxH$_{Mt}$ was co-immunoprecipitated when an isotype control antibody was used, and as expected, EsxH$_{Ms}$ and EsxH$_{Mt}$-H76A E77A were impaired in the interaction with Hrs (Figure 3B and 3C). Interestingly, the co-immunoprecipitation of EsxH$_{Mt}$ and Hrs could only be detected when cells were pre-treated with MG132. Thus, one

possibility is that the EsxG$_{Mt}$-EsxH$_{Mt}$ heterodimer is polyubiquitinated and degraded by the proteasome. In the presence of MG132, the polyubiquitinated species might accumulate, allowing us to detect an interaction between Hrs and an ubiquitinated species of EsxH$_{Mt}$, since Hrs contains an ubiquitin interacting motif (UIM) domain. Arguing against this possibility, when EsxG$_{Mt}$ was co-expressed with EsxH$_{Mt}$, there was little, if any, effect of MG132 on EsxH$_{Mt}$ protein levels (Figure 3A, compare lanes 3 and 7, Figure S4, and Figure S5). In addition, when we examined mono- and polyubiquitinated proteins using the FK2 antibody, inhibition of the proteasome with MG132 caused the accumulation of high molecular weight proteins as anticipated. However, there was no difference seen in the quantity or mobility of EsxH$_{Mt}$ (Figure S5). Further, when we mapped the region of Hrs required for the interaction with EsxG$_{Mt}$-EsxH$_{Mt}$ in the Y2H assay, the UIM domain was not required. Amino acids 398–630, which contain a coiled-coil region, were sufficient to mediate the interaction (Figure 2E). We verified that the C-terminal half of Hrs was sufficient to mediate an interaction by co-immunoprecipitation (Fig. 3D). In summary, these data show that EsxG$_{Mt}$ stabilizes EsxH$_{Mt}$ in the mammalian cytosol and that the heterodimer can bind the C-terminus of Hrs.

To test the hypothesis that the EsxH$_{Mt}$ interaction with Hrs disrupts ESCRT, we examined the effect of EsxG$_{Mt}$ EsxH$_{Mt}$ on epidermal growth factor (EGF) and epidermal growth factor receptor (EGFR) degradation (all performed without MG132 treatment). Upon binding ligand, EGFR is internalized and transferred into ILVs by ESCRT so that it can be degraded upon MVB-lysosome fusion. To determine whether EsxH$_{Mt}$ interferes with this process, we transfected EsxG$_{Mt}$ and EsxH$_{Mt}$ or vector control into HEK293 cells and examined EGFR levels 90 min after EGF treatment. We found that EGFR levels decreased in control cells. In cells co-expressing EsxG$_{Mt}$ and EsxH$_{Mt}$ there was a 63+/−8% (n = 3) increase in the fraction of EGFR that remained undegraded (Figure 3E), similar to what has been seen with Hrs depletion [46]. In contrast, co-expression of EsxG$_{Ms}$ and EsxH$_{Ms}$ had no detectable effect on EGFR degradation (Figure 3E). We observed similar results when we used fluorescent EGF to examine trafficking in A549 cells using fluorescence microscopy. As expected, cells depleted of Hrs showed enhanced EGF fluorescence due to impaired degradation. We observed a similar decreased degradation in cells expressing EsxG$_{Mt}$ and EsxH$_{Mt}$ (Figure 3F and G). In contrast, expression of EsxG$_{Ms}$ EsxH$_{Ms}$ or EsxG$_{Mt}$ EsxH$_{Mt}$-H76A-E77A had little effect on EGF degradation (Figure 3G and 3H). Thus, EsxH$_{Mt}$, in complex with EsxG$_{Mt}$, is sufficient to inhibit EGF and EGFR degradation, an activity that correlates with its binding to Hrs. EsxH$_{Ms}$, from the non-pathogenic species, does not have this property.

EsxG$_{Mt}$ and EsxH$_{Mt}$ arrest phagosome maturation

Because Esx-3 is essential for Mtb growth, we examined the effect of overexpressing EsxH$_{Mt}$ on bacterial trafficking. First, we wanted to determine whether EsxG$_{Mt}$ EsxH$_{Mt}$ could confer a block in maturation to phagosomes containing Msmeg. However, when we expressed EsxG$_{Mt}$ EsxH$_{Mt}$-FLAG under control of the
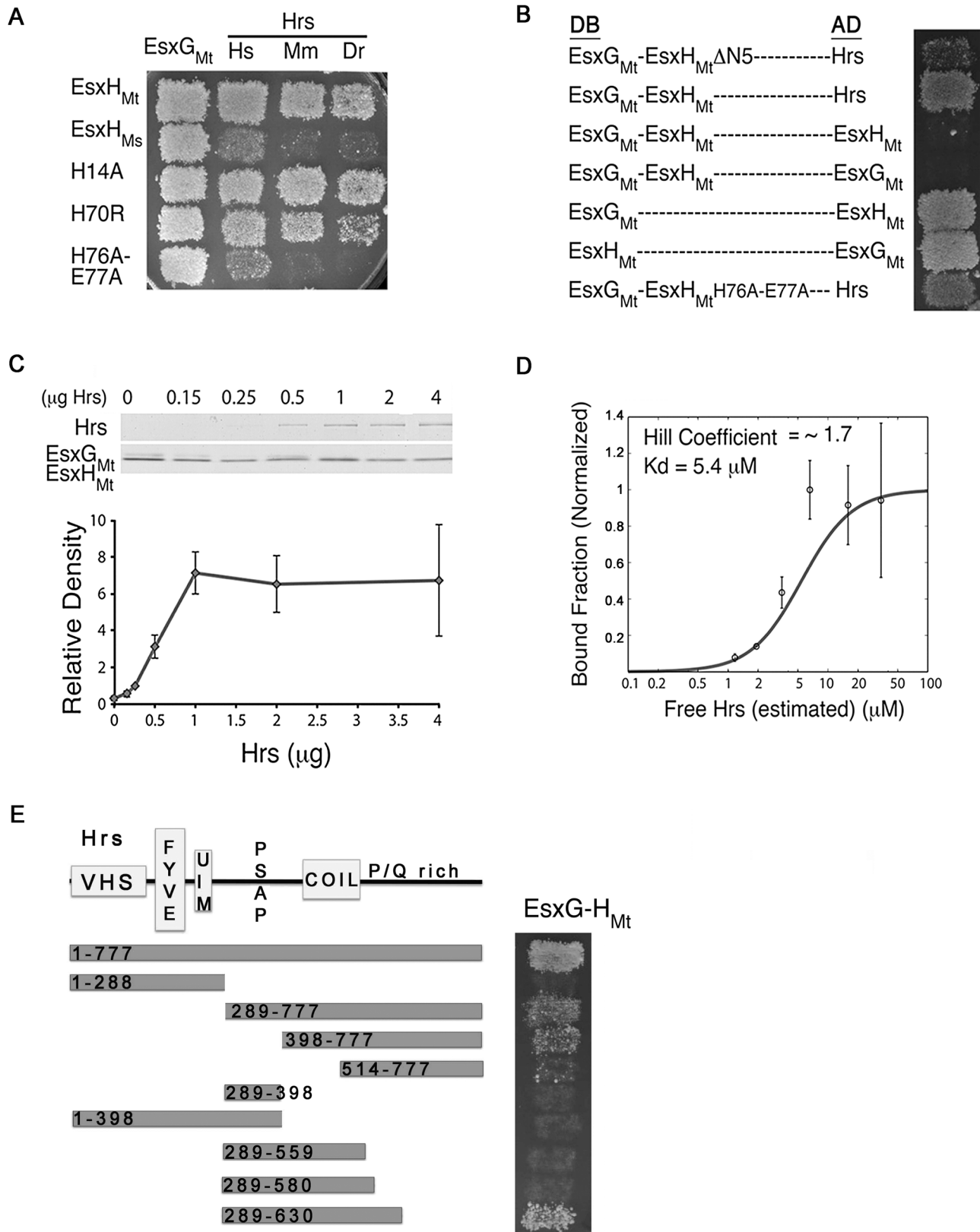
Figure 2. EsxH$_{Mt}$ binds Hrs. (A) Gal4 DNA-binding domain (DB) fusions of EsxH$_{Mt}$, EsxH$_{Ms}$, or mutant EsxH$_{Mt}$ were tested for Y2H interactions with Gal4 activation-domain (AD) fusions of EsxG$_{Mt}$, human (Hs), mouse (Mm), or zebrafish (Dr) Hrs. (B) Y2H interaction between indicated DB and AD constructs. Hrs is human. EsxG$_{Mt}$-EsxH$_{Mt}$-DB did not interact with EsxG$_{Mt}$-AD or EsxH$_{Mt}$-AD, presumably because of the intramolecular interaction in the DB construct. (C) Increasing amounts of Hrs were incubated with a constant amount of immobilized EsxG$_{Mt}$-EsxH$_{Mt}$ and bound fraction examined

hsp60 promoter in Msmeg, it was not secreted (Figure S6). It was secreted by Mtb (Figure 4A), and when we examined whether overexpression of EsxG$_{Mt}$ and EsxH$_{Mt}$-FLAG could enhance phagosome maturation arrest of Mtb, we found less co-localization between Mtb and LAMP1 and enhanced co-localization with TfR with the strain overexpressing EsxH$_{Mt}$-FLAG, compared to a strain transformed with vector control (Figure 4B–E). The defect in lysosomal trafficking was similar to siRNA-mediated silencing of Hrs, Tsg101, and Rab7, and the combination of EsxG$_{Mt}$ EsxH$_{Mt}$ overexpression and ESCRT-silencing resulted in lower LAMP1 co-localization than either manipulation alone (Figure 4B). An Mtb strain that expressed EsxG$_{Mt}$ EsxH$_{Mt}$- H76A-E77A did not exhibit altered trafficking, but the mutant protein also failed to be secreted (Figure 4A, 4F). Mtb did secrete EsxG$_{Ms}$ EsxH$_{Ms}$-FLAG, which, unlike EsxG$_{Mt}$ EsxH$_{Mt}$-FLAG, did not block LAMP1 co-localization (Figure 4A and 4F). We conclude that EsxG$_{Mt}$ EsxH$_{Mt}$, but not EsxG$_{Ms}$ EsxH$_{Ms}$, can prevent lysosomal trafficking during infection, most likely reflecting the ability of EsxH$_{Mt}$ to bind Hrs and impair ESCRT activity.

Discussion

We used high throughput Y2H interactome mapping to identify interactions between secreted Mtb proteins and human proteins, identifying 99 new potential interactions. We made use of a large body of literature that has attempted to catalogue the secretome of Mtb. Our study is subject to the uncertainty around the definition of the Mtb secretome. For example, proteins can be in the culture filtrate due to bacterial lysis, rather than secretion, and bioinformatics predictions may be inaccurate. In addition, many secreted proteins play an intrinsic role in the bacterial lifecycle and are unlikely to make a biologically meaningful interaction with host proteins. Thus, to estimate a false positive hit rate of our system, we included a non-secreted control collection. We found approximately two-fold enrichment in the rate of interactions comparing the secretome collection to the control collection, suggesting that true interactions were identified, but that there also may be a relatively high rate of "pseudo-interactions," which may be valid biophysically but never occur in vivo because the involved proteins are separated spatially or temporally. In addition, the interactome list is by no means complete. We did not screen the entire putative secretome, but rather imposed criteria to try to arrive at a set that was enriched for true secreted proteins likely to play a role in virulence. In addition, the screen was not performed to saturation, and only a fraction of verifiable interactions can be detected by a single method to detect PPIs [31]. Therefore, the list is not comprehensive and likely contains false-positives, but given the paucity of data on host-pathogen interactions in Mtb, it has likely significantly expanded the known Mtb-human protein-protein interactome. It represents a resource for investigators working on Mtb; the confirmation and significance of such interactions will require further validation.

Interactome mapping provides an unbiased strategy to identify host-pathogen interactions for pathogens in which genetic strategies are limited, and it can be complemented by depletion studies in host cells. Such physical interaction mapping can identify redundant or essential factors that may be missed using genetic approaches. For example, in the case of EsxH$_{Mt}$, its importance may have been unrecognized in previous genetic approaches to identify Mtb virulence factors because of redundancy within this large gene family, the existence of additional mechanisms to modulate phagosome maturation, and the essentiality of the Esx-3 system.

This Y2H screen and our previous genome-wide RNAi screen in Drosophila pointed to the importance of the ESCRT machinery in mycobacterial pathogenesis. Here, we show that the ESCRT machinery is important in restricting the intracellular growth of pathogenic mycobacteria, which likely reflects a role of ESCRT in trafficking bacteria to the lysosome, although the effects of ESCRT on endo-lysosomal content and signaling pathways may also play a role. In addition, by modulating the ESCRT machinery, Mtb might alter antigen presentation or exosome formation [42,47].

Further work is required to understand exactly how EsxH$_{Mt}$ impairs ESCRT function. We envision that EsxH$_{Mt}$ inhibits ESCRT on or near the mycobacterial phagosome, where its local concentration would be highest, as opposed to globally disrupting ESCRT. The C-terminal half of Hrs, which we showed binds EsxH$_{Mt}$, has previously been shown to be involved in the interactions with Tsg101 [48,49], STAM [50], and SNAP-25 [45]. Thus, one possibility is that EsxH$_{Mt}$ interferes with these associations. The relatively low affinity measured in vitro between EsxH$_{Mt}$ and Hrs (~5 µM) may be sufficient to disrupt Hrs interactions with other host proteins, as the interactions of Hrs with many of its binding partners are of low affinity [45,48,51,52]. For example, HIV Gag recruits Tsg101 to sites of viral budding by binding the Tsg101 UEV domain with an even lower affinity (K_D~21–50 µM) [48,53]. There may also be a particular form of Hrs or EsxH$_{Mt}$ that exist in vivo in macrophages that exhibits higher affinity. For example, Hrs interacts with the endosomal membrane, engages in numerous protein-protein interactions, and is modified by phosphorylation and ubiquitination, none of which occur when the affinity is measured with recombinant protein. Interestingly MG132, which is known to alter ESCRT activity [54,55], enhanced our ability to detect an interaction between EsxG$_{Mt}$-EsxH$_{Mt}$ and Hrs in co-immunoprecipitation experiments in HEK293 cells. One explanation for the requirement of MG132 to detect the Hrs-EsxH$_{Mt}$ interaction by co-immunoprecipitation may be related to the observation that MG132 impairs ESCRT-dependent trafficking [54,55]. Thus, it is possible that MG132 stabilizes the interaction between EsxH$_{Mt}$ and Hrs by altering ESCRT, although other potential mechanisms could be envisioned. Even in the absence of MG132, EsxG$_{Mt}$-EsxH$_{Mt}$ inhibits ESCRT function. Therefore, we speculate that EsxH$_{Mt}$ preferentially binds to a form of Hrs that exists transiently in cells, a form that is stabilized by MG132. Once bound to Hrs, EsxH$_{Mt}$ could interact with other host proteins that modify Hrs or ESCRT components.

Hrs is one of several host factors that Mtb likely target to create a protected niche [3,4]. Lipoamide dehydrogenase (LpdC) is thought to prevent phagosome-lysosome maturation by retaining the host factor, coronin 1 [29,56]. PtpA, a secreted tyrosine phosphatase, may directly exclude the vacuolar-H$^+$ATPase during infection, impairing acidification and phagosome maturation [27,28,57], while nucleoside diphosphate kinase A (NdkA) targets Rab7 activation [30,58]. In addition, there is less phosphatidylinositol 3-phosphate on the mycobacterial phagosome than latex bead phagosomes, which may reflect the activity of the secreted lipid phosphatase, SapM [59,60]. This leads to impaired recruitment of Hrs [39]. Thus, Hrs activity could be inhibited
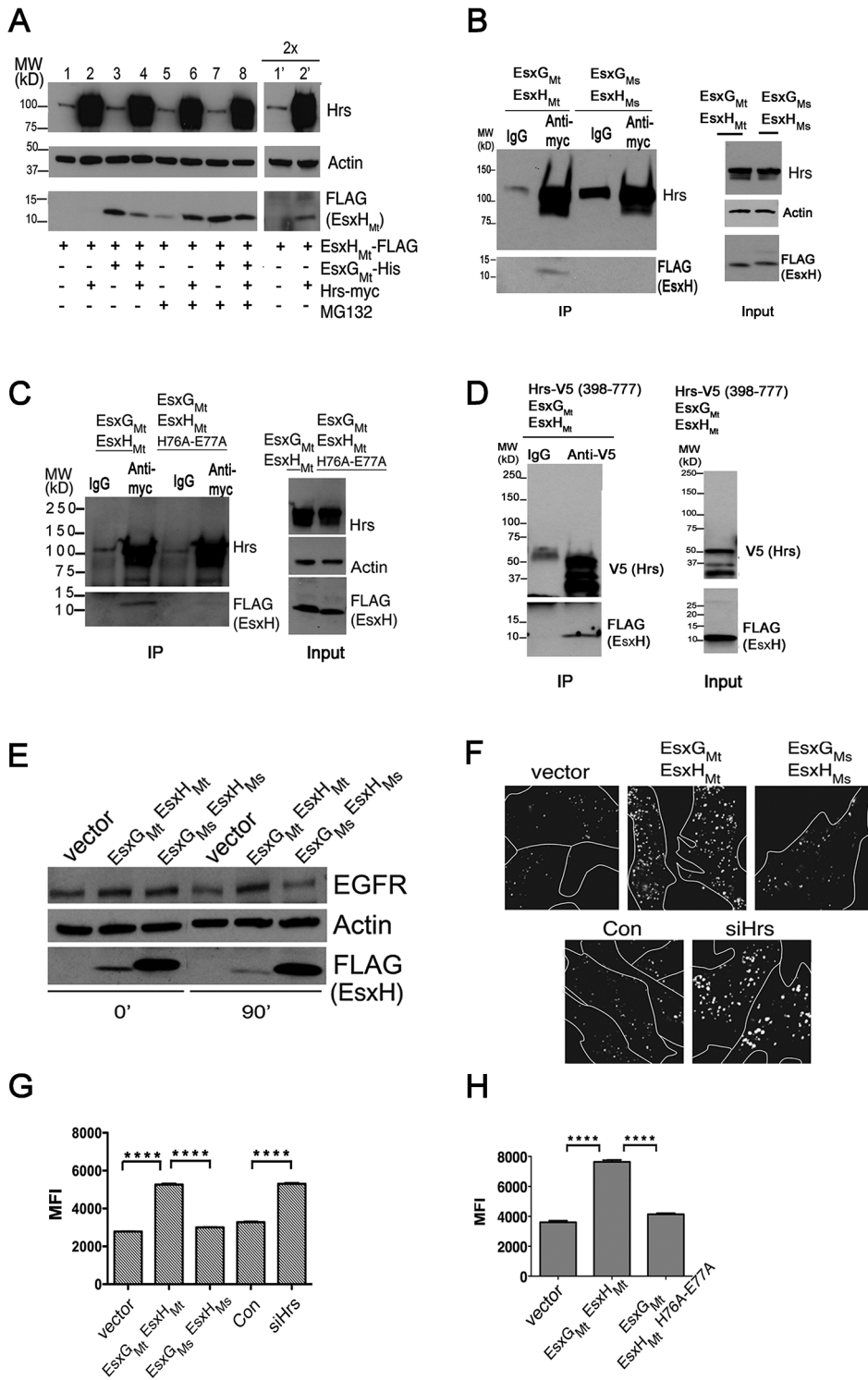
Figure 3. EsxG_Mt and EsxH_Mt interact with Hrs and disrupt ESCRT function in mammalian cells. (A) EsxH_Mt-FLAG, EsxG_Mt-His, and Hrs-myc expressed in HEK293 cells. DMSO or MG132 were added 3 h prior to protein harvest and samples were analyzed by western blotting. Lanes 1′ and 2′ are identical to 1 and 2 except that twice the amount of protein was loaded. Quantification from three independent experiments is shown in Figure S4. (B) Immunoprecipitation (IP) of Hrs using antibody recognizing myc tag or isotype control from HEK293 cells expressing Hrs-myc and either EsxG_Mt-His EsxH_Mt-FLAG or EsxG_Ms-His EsxH_Ms-FLAG. MG132 was used as pre-treatment. Western blot of IP and input were probed with antibodies as indicated. (C) IP of Hrs-myc in HEK293 cells with antibody recognizing myc tag or isotype control from HEK293 cells expressing Hrs-myc, EsxG_Mt-His, and either EsxH_Mt-FLAG or EsxH_Mt-H76A-E77A-FLAG. MG132 was used as pre-treatment. Western blot of IP and input were probed with antibodies as indicated. (D) IP of C-terminal fragment of Hrs (amino acids 398–777) using antibody recognizing V5-tag or isotype control from HEK293 cells expressing Hrs-398–777-V5, EsxG_Mt-His, EsxH_Mt-FLAG. MG132 was used as pre-treatment. Western blot of IP and input were probed with antibodies as indicated. (E) HEK293 cells transfected with indicated plasmids were incubated with EGF for 0 or 90 min prior to western analysis. (F–H) A549 cells transfected with plasmids or siRNAs were imaged 90 min after incubation with Alexa-488 EGF. In F, white lines indicate cell borders. (G) and (H), MFI

of at least 800 endosomes from at least 30 cells. Black bars show mean +/− SEM. ****$p<0.0001$ between indicated conditions, unpaired Student's *t*-test. No MG132 was used in experiments E–H. Data are representative of at least three independent experiments.
doi:10.1371/journal.ppat.1003734.g003

on mycobacterial phagosomes by two synergistic mechanisms: impaired recruitment and direct targeting by EsxH$_{Mt}$. How the activities of these various bacterial effectors are coordinated, whether they are required in concert or function in different cell types or at different time points post-infection, has not been explored. In order to evaluate the relative contribution of the EsxH$_{Mt}$-Hrs interaction to trafficking and intracellular survival during infection, we will have to identify mutations in EsxH$_{Mt}$ that disrupt its binding to Hrs, but that do not interfere with its secretion from Mtb or disrupt bacterial iron acquisition.

It was surprising to us that it was possible to alter Mtb trafficking by overexpressing EsxG$_{Mt}$ EsxH$_{Mt}$, as if Mtb normally expresses a "sub-optimal" amount to maximally alter phagosome maturation. Similarly, ESCRT and Rab7 appear to be sub-maximally inhibited, as further impairing their function by RNAi-mediated silencing also enhances the block in phagosome-lysosome fusion. Given that over-expression of EsxH$_{Mt}$ by Mtb caused a greater effect on trafficking than Hrs silencing (Fig. 4B), EsxH$_{Mt}$ may have additional cellular targets involved in cellular trafficking as well. One explanation for the observation that additional EsxH$_{Mt}$ can further impair trafficking is that this reflects *in vitro* growth conditions, whereas, during infection *in vivo*, EsxH$_{Mt}$ levels may be higher. An additional possibility is that EsxG$_{Mt}$ EsxH$_{Mt}$ production is finely tuned to balance an opposing effect that is detrimental to the bacteria. For example, EsxG$_{Mt}$ and EsxH$_{Mt}$ generate prominent T cell responses, [14,15]. In addition, we found that although the Mtb strain that overexpresses EsxG$_{Mt}$ EsxH$_{Mt}$ exhibited diminished co-localization with LAMP1 and enhanced co-localization with TfR, there was no difference in intracellular growth for this strain relative to control (Figure S7). Thus, overexpression of EsxG$_{Mt}$ EsxH$_{Mt}$, while promoting trafficking, might come with an opposing intracellular fitness cost for bacteria.

In summary, our studies demonstrate that Mtb adapted Esx-3, an ancient microbial system for iron acquisition, to alter host cell physiology. Analogously, Esx-1, which is important for conjugation in Msmeg [61], mediates important host interactions that are critical for virulence, including permeabilizing the mycobacterial phagosome and altering phagosome maturation [5–9,62]. Thus, the duplication and adaptation of TSSSs to new functions appears to be a particularly important evolutionary path to virulence in Mtb. The relatively low affinity between Hrs and its endogenous binding partners may have made it particularly susceptible to manipulation by diverse pathogens, from enveloped viruses to Mtb. The observation that macrophage control of infection is especially sensitive to ESCRT inhibition suggests ESCRT is a likely target of additional pathogens as well.

Materials and Methods

Detailed methods, including description of Y2H interaction mapping, plasmids, siRNAs, and Hill plot analysis, are provided in Text S1.

Tissue culture conditions

RAW264.7 and HEK293 cells were grown in Dulbecco's Modified Eagle Medium (DMEM; Gibco), 20 mM HEPES, 2 mM L-glutamine, and 10% heat inactivated fetal bovine serum (hiFBS; Invitrogen). BMDMs were isolated from C57BL/6 mice as described [63] Penicillin/Streptomycin (Gibco), added

for passaging, was omitted during infections. A549 cells were grown in RPMI 1640 Medium (Gibco), 2 mM L-glutamine, 1× Non-essential Amino Acids (Cellgro), and 10% hiFBS. Cells were grown at 37°C with 5% CO_2 atmosphere. siRNAs were transfected with Hiperfect (Qiagen). Plasmids were transfected into HEK293 cells with Effectene (Qiagen) and A549 cells with Lipofectamine 2000 (Invitrogen).

Bacterial strains and growth conditions

M. tuberculosis H37Rv, *M. bovis*-BCG, and *M. smegmatis* mc^{2}155 were grown at 37°C to log phase in Middlebrook 7H9 media with 0.05% Tween 80, BBL Middlebrook OADC Enrichment, and 0.2% glycerol. Plasmids were selected with 50 µg/ml kanamycin or hygromycin depending upon the resistance marker. To generate EsxG$_{Mt}$ EsxH$_{Mt}$-FLAG and EsxG$_{Ms}$ EsxH$_{Ms}$-FLAG for overexpression in mycobacteria, EsxG-EsxH was amplified from BCG (the EsxG-EsxH region is 100% identical between BCG and Mtb) and Msmeg genomic DNA, respectively, using primers described in Text S1. The PCR products were cloned into pSYMP under control of the *hsp60* promoter [64].

Intracellular bacterial growth assay

RAW cells were seeded one day before infection or they were transfected with siRNAs two days prior to infection with a single cell suspension of Mtb (MOI∼2–5), obtained as previously described [40]. The cells were extensively washed and lysed with 0.2% Triton X-100 3 hpi or 2d later and serial dilutions were plated on 7H10 or 7H11. CFU were calculated 15 to 21 d later.

Lysosomal trafficking assay

RAW cells were transfected with siRNAs for two days and then infected with a single cell suspension of BCG or Mtb (MOI∼20) for 3 h, then washed extensively. Cells were fixed 24 hpi with 4% formaldehyde/PBS for BCG and with 1% paraformaldehyde/PBS overnight for Mtb and immunostained for LAMP1 (Abcam) or TfR (Invitrogen). For Lysotracker (Invitrogen) staining, unfixed RAW cells were incubated with 200 nM Lysotracker, washed twice in PBS, and visualized. Images were captured using the Nikon Eclipse TiE/B automated fluorescent microscope with Photometrics HQ@ Monochrome digital camera. 60× z-stack images were acquired, deconvoluted, and analyzed using NIS-Elements DUO software (see Fig. S3 for details). Contrast was not altered prior to automated image analysis; for reproduced images, alterations were applied equally to all samples.

Recombinant protein binding assay

His-tagged EsxG$_{Mt}$-EsxH$_{Mt}$ was purified as described in Text S1. Prior to inclusion of recombinant proteins in binding reactions they were centrifuged at 100,000× g for 30 min to remove aggregated protein. To determine whether EsxG$_{Mt}$ EsxH$_{Mt}$ binds to Hrs in a direct and saturable manner, 1.0 µg EsxG$_{Mt}$ EsxH$_{Mt}$-6XHis was bound to Ni-NTA beads and incubated with increasing amounts of purified, soluble Hrs (0∼4 µg) in 20 mM HEPES [pH, 7.4], 150 mM KCl, and 0.05% Tween-20, with protease inhibitors (10 mM leupeptin, 1 µg/µL pepstatin, 0.3 mM aprotinin, and 1.74 µg/µL PMSF) for 1 h at 4°C. Beads were washed in PBST (0.1 M PBS 0.05% Tween-20) with 10 mM imidazole. Bound Hrs was analyzed by SDS-PAGE and
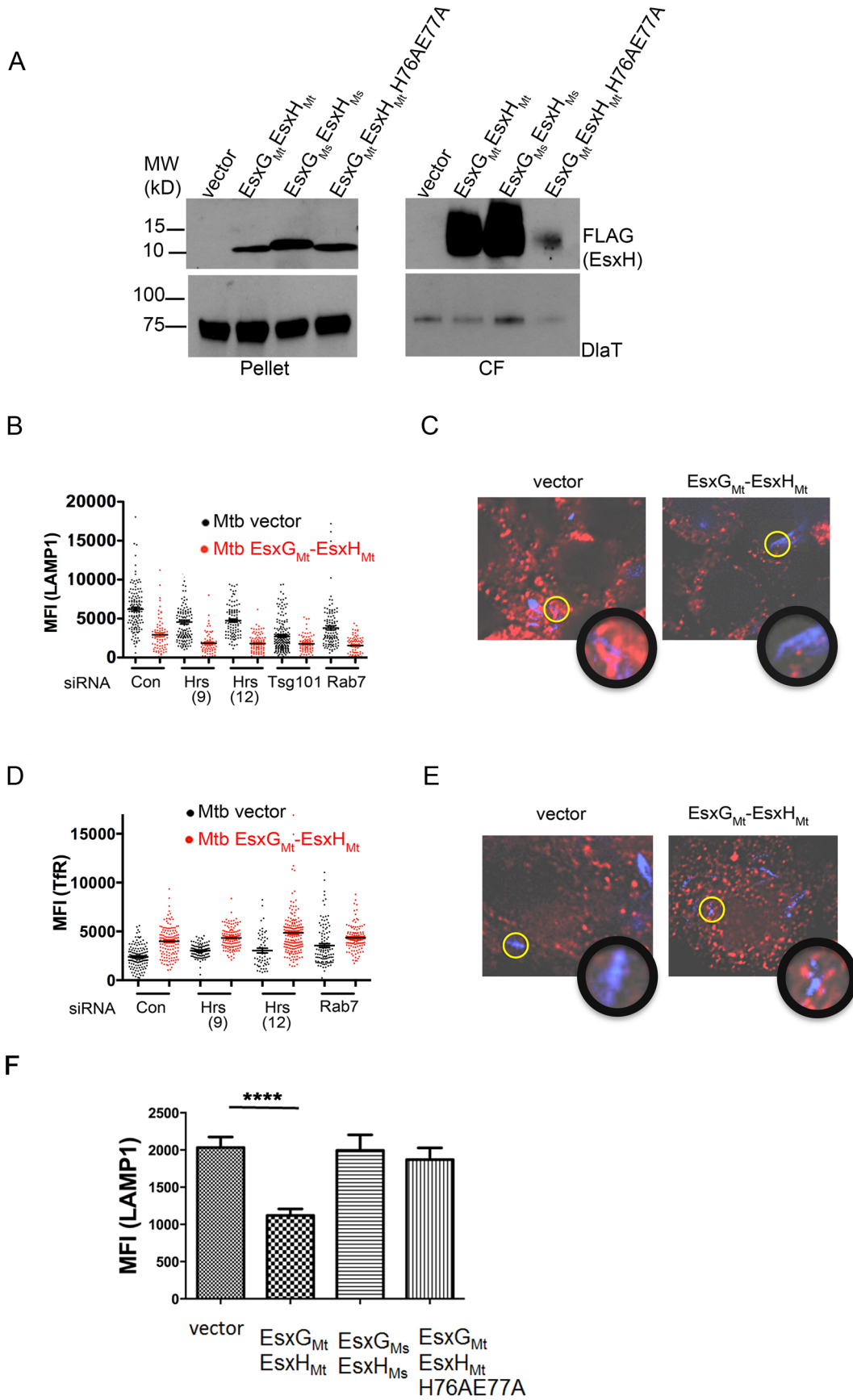
Figure 4. EsxG$_{Mt}$ EsxH$_{Mt}$ arrests phagosome maturation. (A) H37Rv transformed with empty vector, EsxG$_{Mt}$ EsxH$_{Mt}$-FLAG, EsxG$_{Ms}$ EsxH$_{Ms}$-FLAG or EsxG$_{Mt}$ EsxH$_{Mt-}$ H76A-E77A-FLAG were analyzed for the presence of EsxH in the pellet and culture filtrate (CF). DlaT (Rv2215), a cytosolic protein, was used as a loading control and to indicate the degree of bacterial lysis. (B) MFI of phagosomal LAMP1 24 hpi in RAW cells treated with siRNAs and infected with Mtb containing EsxG$_{Mt}$-EsxH$_{Mt}$ plasmid (red) or vector control (black); data points are the mean fluorescence intensity (MFI) around at least 70 phagosomes for each condition; $p<0.0001$ between the two Mtb strains for all conditions, unpaired Student's t-test. (C) Composite images of cells infected with Mtb with autofluorescence of Mtb (blue) and LAMP1 (red). Regions indicated by yellow circles are shown in higher magnification in adjacent panels. (D) MFI of phagosomal TfR 24 hpi in RAW cells treated with siRNAs and infected with Mtb containing EsxG$_{Mt}$-EsxH$_{Mt}$ plasmid (red) or vector control (black); data points are the mean fluorescence intensity (MFI) around at least 50 phagosomes for each condition; $p<0.0001$ between the two Mtb strains for all conditions, except Rab7 ($p = 0.0005$), unpaired Student's t-test. (E) Composite images of cells infected with Mtb with autofluorescence of Mtb (blue) and TfR (red). Regions indicated by yellow circles are shown in higher magnification. (F) MFI of phagosomal LAMP1 in RAW cells infected with Mtb containing the indicated plasmids 24 hpi. Bars show mean +/− SEM. ****$p<0.0001$, unpaired Student's t-test.
doi:10.1371/journal.ppat.1003734.g004

Coomassie staining. Bands were subject to quantification with ImageJ software (v. 1.42).

Co-immunoprecipitation and Western blotting

Cellular lysates were prepared in RIPA buffer with Halt Protease Inhibitor Cocktail (Thermo Scientific) and 10 mM N-ethylmaleimide (Sigma) and analyzed by western blotting. The antibodies used for western analysis are: actin (clone C4/MAB1501, Millipore), Hrs (M79/sc-30221, Santa Cruz Biotechnology), Rab7 (117, Abcam), FLAG (F7425, Sigma), EGFR (#4267S, Cell Signaling), and FK2 (Millipore). For co-immunoprecipitation, HEK293 cells transfected with Hrs-myc and Esx expression plasmids were treated with 20 µM MG132 (Calbiochem) for 3 h prior to mechanical lysis and incubated with Dynabeads Protein G (Novex, Life technologies) pre-bound to isotype control antibody (sc-2025, Santa Cruz Biotechnology), anti-myc antibody (sc-40/9E10, Santa Cruz Biotechnology), or anti-V5 antibody (Invitrogen), and bound proteins were analyzed by western blotting.

EGFR and EGF degradation assays

Two days after transfection, HEK293 cells were incubated in serum-free DMEM and treated with 100 ng/ml of recombinant human EGF (rh-EGF, R&D Systems) essentially as described [65]. Cells were harvested immediately prior to addition of EGF and 90 min later and EGFR analyzed by western blotting. EGF trafficking was assessed similarly to described [66]. Two days after transfection of A549 cells with siRNA or DNA, cells were incubated with serum-free RPMI before addition of 25 µg/ml Alexa Fluor 488-EGF (Invitrogen) in EGF uptake media (RPMI, 2% BSA, 20 mM HEPES) at 4°C for 1 h. Cells were washed to remove unbound ligand, incubated at 37°C for 90 min, and examined by immunofluorescence microscopy.

Mycobacterial secretion of EsxH

To analyze secretion of EsxH$_{Ms}$-FLAG or EsxH$_{Mt}$-FLAG from Mtb and Msmeg, strains were grown to mid-log phase, washed with PBS, and inoculated into Sauton's media. In Sauton's media, they were grown to reach log phase (overnight in the case of Msmeg and for two days in case of Mtb). Thereafter, mycobacteria were pelleted by centrifugation. The supernatants were filtered through 0.22 µM filters followed by precipitation with 12% trichloroacetic acid. The precipitate was washed with ice-cold acetone, air dried, and resuspended in SDS sample buffer. The bacterial pellets were lysed by bead beating in lysis buffer (50 mM Tris-HCl pH 7.5, 5 mM EDTA, 0.6% SDS, 10 mM NaH$_2$PO$_4$, and protease inhibitor) with 0.1 mm zirconia/silica beads (BioSpec Products, Inc.). SDS-sample buffer was added, followed by boiling at 95°C for 5 min. Antibody to the pyruvate

dehydrogenase E2 component sucB (Rv2215/dlaT) [67], a cytosolic protein, was used as a loading control and to indicate the degree of bacterial lysis.

Supporting Information

Dataset S1 Secretome collection screened.
(XLS)

Dataset S2 Control collection screened.
(XLS)

Dataset S3 Y2H interactions between Mtb secretome and human ORFs.
(XLS)

Figure S1 siRNA-mediated depletion of Hrs and Rab7. (A) RAW264.7 (RAW) cells were treated with 50 nM ON-TARGET*plus* individual siRNAs (#9–#12) targeting Hrs or control for 2 d. (B) RAW cells were treated with increasing concentration of siRNA#9 targeting Hrs for 2 or 5 days. (C) A549 cells treated with 50 nM Hrs siRNAs (#12) or control for 2 d. (A)–(C) Western blotting with antibody recognizing Hrs was used to assess silencing. (D) RAW cells were treated with 30 nM siRNA targeting Rab7 or control. Silencing was assessed 2 d later by western blotting using an antibody recognizing Rab7. (E) RAW cells treated with control siRNA (siCON) or siRNA targeting Hrs (#9 or #12) for 2 d were examined by immunofluorescence using antibodies against Hrs, shown in red, and ubiquitinated proteins (FK2) in green.
(TIF)

Figure S2 siRNAs targeting Hrs and Rab7 enhance the intracellular survival of BCG in BMDMs. 4×10^4 BMDMs were transfected with 30 nM siRNA pools targeting Hrs (ON-TARGET*plus*) or Rab7 (siGENOME) 6–8 d after harvest. 3 d later, they were infected with BCG (MOI of 2 to 5). CFU were enumerated 2 days post-infection and are normalized to the average number of CFU in control wells from two independent experiments. Results reflect the mean +/− SEM. *$p<0.05$; **$p<0.01$, unpaired Student's t-test.
(TIF)

Figure S3 Automated image analysis of phagosome maturation (A) For quantifying the degree of co-localization between bacteria and cellular markers or Lysotracker, images were background subtracted and analyzed using the Binary Operation Analysis within NIS Elements Software. Bacteria were selected in the green channel. The region the software has selected that corresponds to the bacteria is shown in red in the second panel. That region was expanded (dilate binary) and then eroded and a binary operation was performed to generate a "donut" in the region surrounding the bacteria. The region of interest (ROI) is shown in purple. The mean fluorescence intensity (MFI) in the

ROI was determined for the cellular marker. Bacteria were analyzed from at least three fields per sample per experiment. We confirmed that automated quantification closely paralleled manual quantification and visual scoring by a blinded observer. (B) To further validate the automated analysis, we verified enhanced LAMP1 co-localization in macrophages pre-treated with IFN-γ, which promotes phagosome maturation [61]. RAW cells treated with control siRNA (siCON) were either pre-treated with IFN-γ or solvent control 24 hours prior to infection with Mtb-GFG. In IFN-γ pre-treated macrophages there is a significant shift in LAMP1 co-localization around bacterial phagosomes 24 hpi. Data points are the MFI of LAMP1 around bacteria; bars show mean +/− SEM; $p<0.0001$. (C) Co-localization of Lamp1, Lysotracker, and TfR with metabolically active BCG compared to co-localization with total BCG. RAW cells were treated with control siRNA (siCON) and infected with BCG constitutively expressing GFP (BCG-GFP) or BCG expressing GFP under a tetracycline inducible promoter (BCG-tet-GFP). AnTc was added 24 hpi to induce expression of GFP. Because it takes >12 h for the strain to become detectably GFP positive, co-localization between BCG-tet-GFP and LAMP1, LysoTracker, or TfR was measured at 48 hpi. For the BCG-GFP strain, LAMP1 and TfR were examined at 48 hpi and LysoTracker at 24 hpi. Data points are the MFI around bacteria; bars show mean +/− SEM; p value of BCG-tet-GFP compared to BCG-GFP for LAMP1 = 0.0081, for LysoTracker <0.0001, for TfR = 0.0046.
(TIF)

Figure S4   Quantification of EsxH$_{Mt}$–FLAG in transfected HEK293 cells. EsxH$_{Mt}$ was co-transfected with vector control, EsxG$_{Mt}$, or Hrs as indicated. Prior to protein harvest, cells were treated with DMSO or MG132. EsxH$_{Mt}$-FLAG levels were quantified from at least three independent experiments using ImageJ software. *$p<0.05$; **$p<0.01$, unpaired Student's t-test; ns-not significant. Whiskers reflect the minimum and maximum data points, while the cross bars show the median.
(TIF)

Figure S5   Treatment with MG132 does not result in higher molecular weight forms of the EsxH proteins. HEK293 cells were transfected with plasmids as indicated. Cells were either treated with DMSO or MG132 prior to protein harvest. Lysates were examined for mono- and polyubiquitinated proteins using the FK2 antibody. The EsxH proteins were visualized using the FLAG antibody. No differences were seen in the mobility of EsxH$_{Mt}$, EsxH$_{Ms}$, or EsxH$_{Mt}$-H76AE77A in the presence of MG132.
(TIF)

Figure S6   EsxG$_{Mt}$ EsxH$_{Mt}$-FLAG is not secreted by Msmeg. Msmeg transformed with empty vector, EsxG$_{Mt}$ EsxH$_{Mt}$-FLAG, or EsxG$_{Ms}$ EsxH$_{Ms}$-FLAG were analyzed for the presence of EsxH in the pellet and culture filtrate (CF). DlaT (Rv2215), a cytosolic protein, was used as a loading control and to indicate the degree of bacterial lysis.
(TIF)

Figure S7   EsxG$_{Mt}$ EsxH$_{Mt}$-FLAG does not alter intracellular growth of Mtb. RAW cells were infected with Mtb containing vector control, EsxG$_{Mt}$ EsxH$_{Mt}$-FLAG, or EsxG$_{Ms}$ EsxH$_{Ms}$-FLAG and bacterial CFU were enumerated at 3 h, 24 h and 48 h post-infection. No statistically significant differences were seen at any time point. Results reflect the mean +/− SEM.
(TIF)

Table S1   Interactions identified between Mtb proteins.
(DOCX)

Table S2   Hit rate by category of Mtb ORFs.
(DOCX)

Text S1   Supporting text. This file contains detailed methods, including description of Y2H interaction mapping, plasmids, siRNAs, and Hill plot analysis.
(DOCX)

Author Contributions

Conceived and designed the experiments: JAP AM AZ VT NS. Performed the experiments: JAP AM AZ VT NS AW MP KP AD DR SK. Analyzed the data: JAP AJB AM AZ VT NS AW MP KP AD DR YK SK. Contributed reagents/materials/analysis tools: DEH MV. Wrote the paper: JAP AM.

References

1. Armstrong JA, Hart PD (1971) Response of cultured macrophages to Mycobacterium tuberculosis, with observations on fusion of lysosomes with phagosomes. J Exp Med 134: 713–740.
2. Russell DG (2001) Mycobacterium tuberculosis: here today, and here tomorrow. Nat Rev Mol Cell Biol 2: 569–577.
3. Flannagan RS, Cosío G, Grinstein S (2009) Antimicrobial mechanisms of phagocytes and bacterial evasion strategies. Nat Rev Microbiol 7: 355–366.
4. Philips JA, Ernst JD (2012) Tuberculosis pathogenesis and immunity. Annu Rev Pathol 7: 353–384.
5. van der Wel N, Hava D, Houben D, Fluitsma D, van Zon M, et al. (2007) M. tuberculosis and M. leprae translocate from the phagolysosome to the cytosol in myeloid cells. Cell 129: 1287–1298.
6. Manzanillo PS, Shiloh MU, Portnoy DA, Cox JS (2012) Mycobacterium tuberculosis activates the DNA-dependent cytosolic surveillance pathway within macrophages. Cell Host Microbe 11: 469–480.
7. Pandey AK, Yang Y, Jiang Z, Fortune SM, Coulombe F, et al. (2009) NOD2, RIP2 and IRF5 play a critical role in the type I interferon response to Mycobacterium tuberculosis. PLoS Pathog 5: e1000500.
8. Hsu T, Hingley-Wilson SM, Chen B, Chen M, Dai AZ, et al. (2003) The primary mechanism of attenuation of bacillus Calmette-Guerin is a loss of secreted lytic function required for invasion of lung interstitial tissue. Proc Natl Acad Sci U S A 100: 12420–12425.
9. Pym AS, Brodin P, Brosch R, Huerre M, Cole ST (2002) Loss of RD1 contributed to the attenuation of the live tuberculosis vaccines Mycobacterium bovis BCG and Mycobacterium microti. Mol Microbiol 46: 709–717.
10. Guinn KM, Hickey MJ, Mathur SK, Zakel KL, Grotzke JE, et al. (2004) Individual RD1-region genes are required for export of ESAT-6/CFP-10 and for virulence of Mycobacterium tuberculosis. Mol Microbiol 51: 359–370.
11. Abdallah AM, Gey van Pittius NC, Champion PA, Cox J, Luirink J, et al. (2007) Type VII secretion–mycobacteria show the way. Nat Rev Microbiol 5: 883–891.
12. Siegrist MS, Unnikrishnan M, McConnell MJ, Borowsky M, Cheng TY, et al. (2009) Mycobacterial Esx-3 is required for mycobactin-mediated iron acquisition. Proc Natl Acad Sci U S A 106: 18792–18797.
13. Serafini A, Boldrin F, Palù G, Manganelli R (2009) Characterization of a Mycobacterium tuberculosis ESX-3 conditional mutant: essentiality and rescue by iron and zinc. J Bacteriol 191: 6340–6344.

14. Hervas-Stubbs S, Majlessi L, Simsova M, Morova J, Rojas MJ, et al. (2006) High frequency of CD4+ T cells specific for the TB10.4 protein correlates with protection against Mycobacterium tuberculosis infection. Infect Immun 74: 3396–3407.

15. Skjøt RL, Brock I, Arend SM, Munk ME, Theisen M, et al. (2002) Epitope mapping of the immunodominant antigen TB10.4 and the two homologous proteins TB10.3 and TB12.9, which constitute a subfamily of the esat-6 gene family. Infect Immun 70: 5446–5453.

16. Sweeney KA, Dao DN, Goldberg MF, Hsu T, Venkataswamy MM, et al. (2011) A recombinant Mycobacterium smegmatis induces potent bactericidal immunity against Mycobacterium tuberculosis. Nat Med 17: 1261–1268.

17. Abdallah AM, Verboom T, Weerdenburg EM, Gey van Pittius NC, Mahasha PW, et al. (2009) PPE and PE_PGRS proteins of Mycobacterium marinum are transported via the type VII secretion system ESX-5. Mol Microbiol 73: 329–340.

18. Bottai D, Di Luca M, Majlessi L, Frigui W, Simeone R, et al. (2012) Disruption of the ESX-5 system of Mycobacterium tuberculosis causes loss of PPE protein secretion, reduction of cell wall integrity and strong attenuation. Mol Microbiol 83(6):1195–209.

19. Abdallah AM, Savage ND, van Zon M, Wilson L, Vandenbroucke-Grauls CM, et al. (2008) The ESX-5 secretion system of Mycobacterium marinum modulates the macrophage response. J Immunol 181: 7166–7175.

20. Katzmann DJ, Odorizzi G, Emr SD (2002) Receptor downregulation and multivesicular-body sorting. Nat Rev Mol Cell Biol 3: 893–905.

21. Raiborg C, Stenmark H (2009) The ESCRT machinery in endosomal sorting of ubiquitylated membrane proteins. Nature 458: 445–452.

22. Rual JF, Venkatesan K, Hao T, Hirozane-Kishikawa T, Dricot A, et al. (2005) Towards a proteome-scale map of the human protein-protein interaction network. Nature 437: 1173–1178.

23. Venkatesan K, Rual JF, Vazquez A, Stelzl U, Lemmens I, et al. (2009) An empirical framework for binary interactome mapping. Nat Methods 6: 83–90.

24. Lightbody KL, Renshaw PS, Collins ML, Wright RL, Hunt DM, et al. (2004) Characterisation of complex formation between members of the Mycobacterium tuberculosis complex CFP-10/ESAT-6 protein family: towards an understanding of the rules governing complex formation and thereby functional flexibility. FEMS Microbiol Lett 238: 255–262.

25. Lightbody KL, Ilghari D, Waters LC, Carey G, Bailey MA, et al. (2008) Molecular features governing the stability and specificity of functional complex formation by Mycobacterium tuberculosis CFP-10/ESAT-6 family proteins. J Biol Chem 283: 17681–17690.

26. McMath LM, Habel JE, Sankaran B, Yu M, Hung LW, et al. (2010) Crystallization and preliminary X-ray crystallographic analysis of a Mycobacterium tuberculosis ferritin homolog, BfrB. Acta Crystallogr Sect F Struct Biol Cryst Commun 66: 1657–1661.

27. Wong D, Bach H, Sun J, Hmama Z, Av-Gay Y (2011) Mycobacterium tuberculosis protein tyrosine phosphatase (PtpA) excludes host vacuolar-H+ -ATPase to inhibit phagosome acidification. Proc Natl Acad Sci U S A 108: 19371–19376.

28. Bach H, Papavinasasundaram KG, Wong D, Hmama Z, Av-Gay Y (2008) Mycobacterium tuberculosis virulence is mediated by PtpA dephosphorylation of human vacuolar protein sorting 33B. Cell Host Microbe 3: 316–322.

29. Deghmane AE, Soualhine H, Soulhine H, Bach H, Sendide K, et al. (2007) Lipoamide dehydrogenase mediates retention of coronin-1 on BCG vacuoles, leading to arrest in phagosome maturation. J Cell Sci 120: 2796–2806.

30. Sun J, Wang X, Lau A, Liao TY, Bucci C, et al. (2010) Mycobacterial nucleoside diphosphate kinase blocks phagosome maturation in murine RAW 264.7 macrophages. PLoS ONE 5: e8769.

31. Yu H, Braun P, Yildirim MA, Lemmens I, Venkatesan K, et al. (2008) High-quality binary protein interaction map of the yeast interactome network. Science 322: 104–110.

32. Master SS, Rampini SK, Davis AS, Keller C, Ehlers S, et al. (2008) Mycobacterium tuberculosis prevents inflammasome activation. Cell Host Microbe 3: 224–232.

33. Lange S, Perera S, Teh P, Chen J (2012) Obscurin and KCTD6 regulate cullin-dependent small ankyrin-1 (sAnk1.5) protein turnover. Mol Biol Cell 23: 2490–2504.

34. Hubner M, Peter M (2012) Cullin-3 and the endocytic system: New functions of ubiquitination for endosome maturation. Cell Logist 2: 166–168.

35. Watson RO, Manzanillo PS, Cox JS (2012) Extracellular M. tuberculosis DNA Targets Bacteria for Autophagy by Activating the Host DNA-Sensing Pathway. Cell 150: 803–815.

36. Thurston TL, Ryzhakov G, Bloor S, von Muhlinen N, Randow F (2009) The TBK1 adaptor and autophagy receptor NDP52 restricts the proliferation of ubiquitin-coated bacteria. Nat Immunol 10: 1215–1221.

37. Shembade N, Harhaj NS, Liebl DJ, Harhaj EW (2007) Essential role for TAX1BP1 in the termination of TNF-alpha-, IL-1- and LPS-mediated NF-kappaB and JNK signaling. EMBO J 26: 3910–3922.

38. Quinton LJ, Mizgerd JP (2011) NF-κB and STAT3 signaling hubs for lung innate immunity. Cell Tissue Res 343: 153–165.

39. Vieira OV, Harrison RE, Scott CC, Stenmark H, Alexander D, et al. (2004) Acquisition of Hrs, an essential component of phagosomal maturation, is impaired by mycobacteria. Mol Cell Biol 24: 4593–4604.

40. Philips JA, Rubin EJ, Perrimon N (2005) Drosophila RNAi screen reveals CD36 family member required for mycobacterial infection. Science 309: 1251–1253.

41. Philips JA, Porto MC, Wang H, Rubin EJ, Perrimon N (2008) ESCRT factors restrict mycobacterial growth. Proc Natl Acad Sci U S A 105: 3070–3075.

42. Henne WM, Buchkovich NJ, Emr SD (2011) The ESCRT pathway. Dev Cell 21: 77–91.

43. Ilghari D, Lightbody KL, Veverka V, Waters LC, Muskett FW, et al. (2011) Solution structure of the Mycobacterium tuberculosis EsxG·EsxH complex: functional implications and comparisons with other M. tuberculosis Esx family complexes. J Biol Chem 286: 29993–30002.

44. Callahan B, Nguyen K, Collins A, Valdes K, Caplow M, et al. (2010) Conservation of structure and protein-protein interactions mediated by the secreted mycobacterial proteins EsxA, EsxB, and EspA. J Bacteriol 192: 326–335.

45. Tsujimoto S, Bean AJ (2000) Distinct protein domains are responsible for the interaction of Hrs-2 with SNAP-25. The role of Hrs-2 in 7 S complex formation. J Biol Chem 275: 2938–2942.

46. Lu Q, Hope LW, Brasch M, Reinhard C, Cohen SN (2003) TSG101 interaction with HRS mediates endosomal trafficking and receptor down-regulation. Proc Natl Acad Sci U S A 100: 7626–7631.

47. Wegner CS, Rodahl LM, Stenmark H (2011) ESCRT proteins and cell signalling. Traffic 12: 1291–1297.

48. Pornillos O, Higginson DS, Stray KM, Fisher RD, Garrus JE, et al. (2003) HIV Gag mimics the Tsg101-recruiting activity of the human Hrs protein. J Cell Biol 162: 425–434.

49. Bouamr F, Houck-Loomis BR, De Los Santos M, Casaday RJ, Johnson MC, et al. (2007) The C-terminal portion of the Hrs protein interacts with Tsg101 and interferes with human immunodeficiency virus type 1 Gag particle production. J Virol 81: 2909–2922.

50. Asao H, Sasaki Y, Arita T, Tanaka N, Endo K, et al. (1997) Hrs is associated with STAM, a signal-transducing adaptor molecule. Its suppressive effect on cytokine-induced cell growth. J Biol Chem 272: 32785–32791.

51. Mayers JR, Fyfe I, Schuh AL, Chapman ER, Edwardson JM, et al. (2011) ESCRT-0 assembles as a heterotetrameric complex on membranes and binds multiple ubiquitinylated cargoes simultaneously. J Biol Chem 286: 9636–9645.

52. Bean AJ, Davanger S, Chou MF, Gerhardt B, Tsujimoto S, et al. (2000) Hrs-2 regulates receptor-mediated endocytosis via interactions with Eps15. J Biol Chem 275: 15271–15278.

53. Im YJ, Kuo L, Ren X, Burgos PV, Zhao XZ, et al. (2010) Crystallographic and functional analysis of the ESCRT-I/HIV-1 Gag PTAP interaction. Structure 18: 1536–1547.

54. Longva KE, Blystad FD, Stang E, Larsen AM, Johannessen LE, et al. (2002) Ubiquitination and proteasomal activity is required for transport of the EGF receptor to inner membranes of multivesicular bodies. J Cell Biol 156: 843–854.

55. Melikova MS, Kondratov KA, Kornilova ES (2006) Two different stages of epidermal growth factor (EGF) receptor endocytosis are sensitive to free ubiquitin depletion produced by proteasome inhibitor MG132. Cell Biol Int 30: 31–43.

56. Ferrari G, Langen H, Naito M, Pieters J (1999) A coat protein on phagosomes involved in the intracellular survival of mycobacteria. Cell 97: 435–447.

57. Sturgill-Koszycki S, Schlesinger PH, Chakraborty P, Haddix PL, Collins HL, et al. (1994) Lack of acidification in Mycobacterium phagosomes produced by exclusion of the vesicular proton-ATPase. Science 263: 678–681.

58. Sun J, Deghmane AE, Soualhine H, Hong T, Bucci C, et al. (2007) Mycobacterium bovis BCG disrupts the interaction of Rab7 with RILP contributing to inhibition of phagosome maturation. J Leukoc Biol 82: 1437–1445.

59. Vergne I, Chua J, Lee HH, Lucas M, Belisle J, et al. (2005) Mechanism of phagolysosome biogenesis block by viable Mycobacterium tuberculosis. Proc Natl Acad Sci U S A 102: 4033–4038.

60. Purdy GE, Owens RM, Bennett L, Russell DG, Butcher BA (2005) Kinetics of phosphatidylinositol-3-phosphate acquisition differ between IgG bead-containing phagosomes and Mycobacterium tuberculosis-containing phagosomes. Cell Microbiol 7: 1627–1634.

61. Coros A, Callahan B, Battaglioli E, Derbyshire KM (2008) The specialized secretory apparatus ESX-1 is essential for DNA transfer in Mycobacterium smegmatis. Mol Microbiol 69: 794–808.

62. MacGurn JA, Cox JS (2007) A genetic screen for Mycobacterium tuberculosis mutants defective for phagosome maturation arrest identifies components of the ESX-1 secretion system. Infect Immun 75: 2668–2678.

63. Banaiee N, Kincaid EZ, Buchwald U, Jacobs WR, Jr., Ernst JD (2006) Potent inhibition of macrophage responses to IFN-gamma by live virulent Mycobacterium tuberculosis is independent of mature mycobacterial lipoproteins but dependent on TLR2. J Immunol 176: 3019–3027.

64. Festa RA, McAllister F, Pearce MJ, Mintseris J, Burns KE, et al. (2010) Prokaryotic ubiquitin-like protein (Pup) proteome of Mycobacterium tuberculosis [corrected] . PLoS One 5: e8589.

65. Stern KA, Place TL, Lill NL (2008) EGF and amphiregulin differentially regulate Cbl recruitment to endosomes and EGF receptor fate. Biochem J 410: 585–594.

66. Liang C, Lee JS, Inn KS, Gack MU, Li Q, et al. (2008) Beclin1-binding UVRAG targets the class C Vps complex to coordinate autophagosome maturation and endocytic trafficking. Nat Cell Biol 10: 776–787.

67. Venugopal A, Bryk R, Shi S, Rhee K, Rath P, et al. (2011) Virulence of Mycobacterium tuberculosis depends on lipoamide dehydrogenase, a member of three multienzyme complexes. Cell Host Microbe 9: 21–31.